EES Catalysis

PAPER

View Article Online
View Journal

Cite this: DOI: 10.1039/d6ey00026f

Ionic liquid catalyzes reactive CO_2 capture

Rohan Sartape,[a] Rashmi Mishra,[b] Vamsi V. Gande,[a] Sophia Johnson,[a] Bianca Berry,[c] Ishaku Amos,[a] Rohit Chauhan,[a] Amey Thorat,[b] Jindal K. Shah[b] and Meenesh R. Singh*[a]

CO_2 hydroxylation is the underlying reaction for a wide range of reactive CO_2 capture (RCC) techniques. Despite being thermodynamically favorable, CO_2 hydroxylation kinetics are sluggish due to a higher energy barrier associated with bending the linear CO_2 molecule before nucleophilic attack by OH^-. Here, we report a previously unrecognized catalytic effect in which ionic liquids (ILs) increase the rates of CO_2 hydroxylation by pre-activating (or bending) CO_2 locally around the IL. ILs are known for their higher CO_2 solubilities due to their larger void fractions; however, their role in catalyzing the CO_2 hydroxylation reaction, an important step in RCC, has not been reported previously. NMR and FTIR measurements, together with quantum-chemical calculations, are consistent with bicarbonate being the dominant stable species, while carbonate appears to revert to bicarbonate over time under the studied conditions. For instance, the addition of BMIM NTf_2 to a KOH-ethylene glycol mixture accelerates CO_2 hydroxylation by sixfold by lowering the activation energy (~33%) without chemically binding CO_2, highlighting its catalytic role. Isotope-labeled ATR-FTIR experiments confirm enhanced CO_2 bending in ionic liquids through the appearance of a hot band, indicative of increased population of thermally accessible bent vibrational states. While low IL loadings enhance kinetics, higher concentrations hinder CO_2 mass transfer due to reduced interfacial tension. The nature of IL cation and anion strongly influences rates, with shorter alkyl chains and I^-/OTf^- anions providing the highest activity. The system demonstrates reversibility and robustness under anhydrous flue gas conditions, offering a tunable pathway for efficient CO_2 capture.

Received 6th February 2026,
Accepted 26th March 2026

DOI: 10.1039/d6ey00026f

rsc.li/eescatalysis

Broader context

The escalating need to mitigate anthropogenic CO_2 emissions has driven intense efforts to develop capture technologies that are both energy-efficient and scalable. Conventional amine-based processes, while widely deployed, suffer from high energy requirements for regeneration, volatility, and corrosivity, underscoring the need for sustainable alternatives. Ionic liquids (ILs) and deep eutectic solvents (DESs) offer promise due to their tunable properties, low volatility, and strong CO_2 solubility, yet practical limitations such as high viscosity and slow mass transfer have hindered large-scale adoption. This study demonstrates a new concept: ILs can act as catalysts for CO_2 hydroxylation, promoting bicarbonate formation through molecular pre-activation rather than direct binding. Using NMR, FTIR, and quantum-chemical simulations, we show that ILs bend and activate CO_2, significantly lowering the activation energy for hydroxylation while maintaining reversibility. The catalytic effect is strongly influenced by IL structure, with cation alkyl chain length and anion chemistry dictating efficiency and stability, thereby offering rational design principles for optimized capture systems. By revealing IL-catalyzed hydroxylation as a tunable and scalable mechanism, this work provides critical molecular-level insights and positions IL-based systems as viable, energy-efficient alternatives to amines. The findings establish a foundation for advancing next-generation solvent systems that can overcome current bottlenecks in sustainable carbon capture.

1. Introduction

Addressing global warming remains a critical goal of the 21st century, driving U.S. Department of Energy initiatives like Carbon Negative Shots to advance the development of novel CO_2 capture technologies.[1–4] Amine-based systems have long dominated the field due to their effectiveness, even in the presence of impurities, through chemisorption the forms carbamates.[5–8] The structure of amines significantly impacts absorption capacity, regeneration energy, and kinetics.[9–13] However, the energy penalty for regeneration, corrosivity, and high vapor pressure properties of amines cannot be ignored, which has become a significant concern for industries lately.[14–17] With a growing demand for environmental

[a] Department of Chemical Engineering, University of Illinois Chicago, 929 W. Taylor St., Chicago, 60607, Illinois, USA. E-mail: mrsingh@uic.edu; Tel: +1 312-996-3424
[b] School of Chemical Engineering, Oklahoma State University, Stillwater, 74078, Oklahoma, USA
[c] Lyons Township High School, Western Springs, 60558, IL, USA

remediation, industries and organizations are increasingly turning to novel technologies.[18–21] We acknowledge that comprehensive techno-economic analyses comparing emerging solvents to industrial amine systems remain limited. Nevertheless, preliminary life-cycle assessments (LCA) and TEA studies often serve as critical enablers for early-stage funding announcements and pilot-scale deployment.[22–24]

Ionic liquids (ILs) offer high CO_2 capacity, tunable chemistry, and negligible vapor pressure.[25–27] However, their high viscosity can severely limit CO_2 mass transfer[13] and challenges in synthesis and scalability further constrain their practical deployment.[28–31] Although aprotic heterocyclic anions (AHAs) are available that can react with CO_2, they are often described as "lower-viscosity" relative to many CO_2-reactive ILs (~3–20 mPa s for AHAs,[32] ~300–400 mPa s for acetate-based ILs at 313 K). They are not yet commercially available, making a comprehensive techno-economic analysis difficult, if not impossible.[33–35] Furthermore, the viscosities of AHAs remain slightly higher than those of industrial aqueous amines, such as 30 wt% MEA (~2–3 cP at 313 K), which can impose additional mass-transfer and pumping penalties. Deep eutectic solvents, an alternative to ILs for CO_2 capture, are formed by combining a hydrogen bond acceptor (HBA) and a hydrogen bond donor (HBD), resulting in a mixture with a melting point lower than that of the individual components.[36–38] At a certain molar ratio (typically 1 : 1, 1 : 2 or 2 : 1) of HBA to HBD, the melting point of the DES can be reduced significantly lower than that at the eutectic composition, enabling their applications at room temperature. DES inherits almost all the advantages of IL but offers lower production costs and ease of synthesis.[39–41] Alkaline DES, composed of an alkaline salt as the HBA (*e.g.*, potassium hydroxide) and an HBD (*e.g.*, ethylene glycol), has demonstrated excellent CO_2 capture performance.[42–44]

Recent studies from our group demonstrated that alkaline DES can achieve CO_2 capture rates as high as 0.13 mmol m^{-2} s^{-1} with regeneration energies of 120 kJ mol^{-1} of captured CO_2, using a pH-swing process.[45–49] Mishra *et al.*[50] investigated various intermolecular interactions involved in alkaline DES, comprised of ethylene glycol (EG) and KOH, to understand its enhanced performance in CO_2 capture. Using FTIR and quantum chemical analyses, noncovalent interactions and structural changes were found to be critical for optimizing DES design for direct-air-capture applications. In parallel, mixing DESs with ILs (DES–IL) has been proposed to reduce energy losses in electrochemical CO_2 capture.[51,52] Our group observed a non-monotonic ionic conductivity behavior in various EG–IL mixtures as a function of concentration, attributed to ion pair aggregation that limits charge mobility[53,54] and was linked to the extent of ion fluctuations in the first solvation shell of a given ion.[55] Although the physicochemical properties of alkaline DES–IL mixtures have begun to be investigated, CO_2 chemisorption kinetics in DES–IL mixtures remain unexplored and present an important avenue for future research.

In general, hydroxylation reactions with CO_2 require prior CO_2 activation and high activation energy, due to its linear, symmetric structure and chemical inertness. Increasing the temperature can facilitate activation but is often energy-intensive, making the use of activation agents/catalysts such as N-heterocyclic carbenes, polyoxometalates, and ILs essential.[56,57] ILs, through electrostatic interactions, can interact with CO_2.[51,58–63] It is well established that the solvation effect and solvation energy in CO_2 hydroxylation play a crucial role.[64,65] Iida *et al.* demonstrated that CO_2 hydroxylation in the gas phase is barrierless. However, in the aqueous phase, the reaction exhibits a significant activation barrier of 54 kJ mol^{-1}. Their work further revealed that CO_2 hydroxylation involves the desolvation of the hydroxide moiety, and the oxygen atom of CO_2 increasingly attracts solvent molecules as the reaction coordinate decreases.[64] In a similar vein, the presence of IL can modulate the solution energies around the hydroxide moiety and the O atom of CO_2. This altered energy landscape facilitates CO_2 bending and lowers the effective energy barrier, thereby catalyzing the CO_2 capture process. A schematic illustration of the phenomena is also presented in Fig. 1. In an aqueous medium, the formation of bicarbonate or carbonate products from the hydroxylation of CO_2 is strongly governed by how efficiently water can transfer protons and stabilize transition states.[66] Since ILs and DES usually have trace amounts of water, products can remain in bicarbonate form, which is advantageous.[67,68] Such a concept is also widely recognized in catalysis, where modulation of solvation energy plays a crucial role in lowering activation barriers. Various areas of chemistry leverage solvation-energy tuning to enhance reaction rates, including enzymatic catalysis[69,70] and confined nanocage catalysis.[71,72] A notable biological example is the enzyme carbonic anhydrase (CA), which catalyzes the hydration of CO_2 in mammalian systems. The catalytic cycle of CA involves the deprotonation of a coordinated water molecule to generate a nucleophilic hydroxide species that subsequently attacks CO_2 to form bicarbonate.[73] Inspired by this mechanism, CA has also been explored in combination with amine solutions to enhance CO_2 capture rates.[74,75] However, the large-scale deployment of enzyme-assisted systems remains challenging due to the high

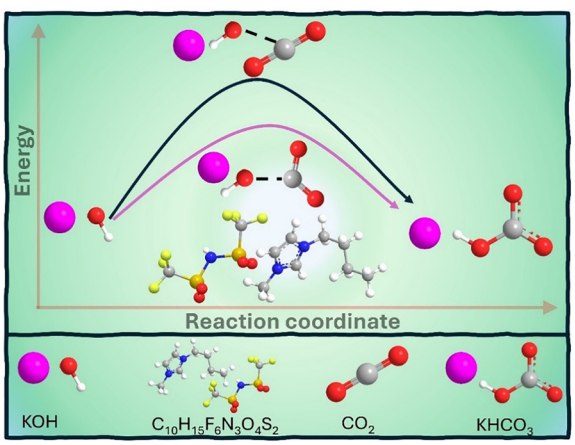

Fig. 1 Schematic illustration of CO_2 hydroxylation with and without IL.

cost and stability limitations associated with enzyme production and operation.[76]

Building on these principles, DESs have been explored as potential catalysts or activation agents for various reactions,[77,78] offering sustainability and tunability.[79–81] Similarly, IL–solvent mixtures, particularly at low ionic liquid mole fractions ($x_{IL} \leq 0.05$), exhibit enhanced chemical activity compared to concentrated IL systems.[82–92] For example, Man *et al.*[82] reported maxima in substitution reaction rates ($x_{IL} = 0.02$) for 1-butyl-3-methylimidazolium bis(trifluorosulfonyl)imide (BMIM NTf_2), attributing this to microscopic interactions that influence the transition state. Zhang *et al.*[93] demonstrated that free $BMIM^+$ cations impact the hydroxylation rate of 2-methylcyclohexanone *via* ionic mechanisms. Similarly, Gilbert *et al.*[89] reported enhanced nucleophilic substitution rates using small amounts of BMIM NTf_2 without affecting stereoselectivity. Kochly *et al.*[92] further highlighted that IL-induced rate enhancements in elimination reactions depend on the hydrogen-bonding properties of the solvent and the steric effects of the IL anion.

Herein, we demonstrate that an alkaline DES–IL mixture (specifically, KOH, ethylene glycol (EG), and IL) enhances CO_2 capture by facilitating its conversion to a bicarbonate species. Due to the alkalinity of the system, an interplay between bicarbonate and carbonate species occurs, facilitated by *in situ* water formation during the CO_2 capture process. To elucidate the reaction mechanism of IL-catalyzed CO_2 capture, we systematically varied the IL concentration in DES–IL mixtures and observed the impact on the CO_2 capture performance. Finally, to understand the role of IL structure, we screened various DES–IL combinations to evaluate the influence of both cation and anion chemistry on CO_2 uptake. This study underscores the potential of DES–IL systems as a cost-effective, tunable platform for efficient CO_2 capture and offers insight for the rational design of next-generation carbon capture technologies.

We also acknowledge that, in the field of CO_2 capture, promoter species such as piperazine are widely used to enhance kinetics by increasing the rate of CO_2 hydration in systems such as tertiary amines or K_2CO_3.[94–97] In the present work, however, our spectroscopic observations and mechanistic analysis indicate that the enhancement observed includes catalytic contributions rather than solely conventional promoter behavior.

2. Results and discussion

2.1. Determination of reaction species and reaction pathway

2.1.1. Experimental NMR and quantum-chemical calculations. To identify the reaction species and pathways involved in CO_2 absorption in DES and DES–IL mixtures, nuclear magnetic resonance (NMR) experiments were conducted in deuterated dimethyl sulfoxide (DMSO-d_6) solvent at 25 °C. Chemical species involved in the CO_2 chemisorption are shown in Fig. 2(a), *viz.* EG, IL (BMIM NTf_2), bicarbonate, carbonate, and a complex of CO_2 and EG^-. Fig. 2(b) shows the ^{13}C NMR data for DES and DES–IL mixture bubbled with $^{13}CO_2$ gas at different time intervals. The IL chosen for the study is BMIM NTf_2, which has shown some catalytic activity as discussed previously,[82,93] and DES is EG with KOH, which has been previously used for the pH-swing CO_2 capture process.[48,54] Additional details about the experiment are provided in Section S1 of the supplementary information (SI).

For the system containing DES, bubbling $^{13}CO_2$ for 2 minutes, results in the appearance of new resonance peaks at 61, 67, 159, and 167 ppm. Furthermore, as time increases, these peaks appear to increase in intensity except for 167 ppm, which shifts upfield and decreases in intensity. Peaks at 159 and 167 ppm, labelled as α and β, can be ascribed to bicarbonate and carbonate species involved in the EG-KOH system. NMR signals from mixing isotope-labelled 0.1 M sodium bicarbonate and sodium carbonate with EG-KOH are also shown in Fig. S1 to validate the assigned peaks. The increase in the bicarbonate peak at 159 ppm over time, along with its stable chemical shift, coupled with the gradual decrease and downfield shift of the carbonate peak at 167 ppm, suggest that both species form at the beginning of the reaction. After 2 minutes of bubbling CO_2 through the DES system, the carbonate peak begins to decrease in intensity, while the bicarbonate peak continues to increase. This indicates that carbonate progressively regenerates into bicarbonate. The process is analogous to the well-established pH-driven equilibrium dynamics of CO_2 when dissolved in water.[98] A tiny peak, labelled as δ, is also observed at 160.9 ppm after 8 minutes of $^{13}CO_2$ bubbling. This peak is ascribed to the CO_2 attached to the deprotonated ethylene glycol, as shown in Fig. 2(a). A similar set of new peaks at 61, 67, 159, and 167 ppm is again observed in the system containing BMIM NTf_2 mixed with DES in Fig. 2(b). A comparison of normalized signal intensity at 159 ppm in Fig. S2 reveals an accelerated conversion to bicarbonate in the presence of BMIM NTf_2. Furthermore, after 8 minutes of bubbling with $^{13}CO_2$, a signal at 124 ppm corresponding to dissolved CO_2 appears, indicating the completion of the chemisorption process.

In experiments with DES and DES–IL mixtures, resonance peaks at 61 and 67 ppm also increase with time and are ascribed to the methylene groups of the hydroxy ethyl carbonate (HEC) labelled as 2 and 3, as shown in Fig. 2(b).[99] Such a characteristic peak indicates the attack of the deprotonated form of EG on CO_2.[99–101] Cui *et al.*[99] observed that for a CO_2 absorption system containing azolide-based ILs, instead of the formation of carbamate species by reacting with azolide ions, the CO_2 reacts with the –OH group of ethylene glycol to form the carbonate species. Zhou *et al.*[101] observed a similar reaction product when EG reacted with K_2CO_3. Based on their observations, the overall equilibrium reaction involves the reaction of carbonate and EG to form a hydroxide ion and $HO–CH_2–CH_2–O–COO^-$. Based on their analysis, reaction pathways were proposed that involved the formation of bicarbonate, carbonate, water, and carbonic acid. Other published works also indicate that CO_2 binds to the EG molecule following its deprotonation.[36,102] These studies indicate that CO_2 absorption in alkaline DES involves deprotonation of EG and formation of $HO–CH_2–CH_2–O–COO^-$ (HEC), which is also a feasible pathway

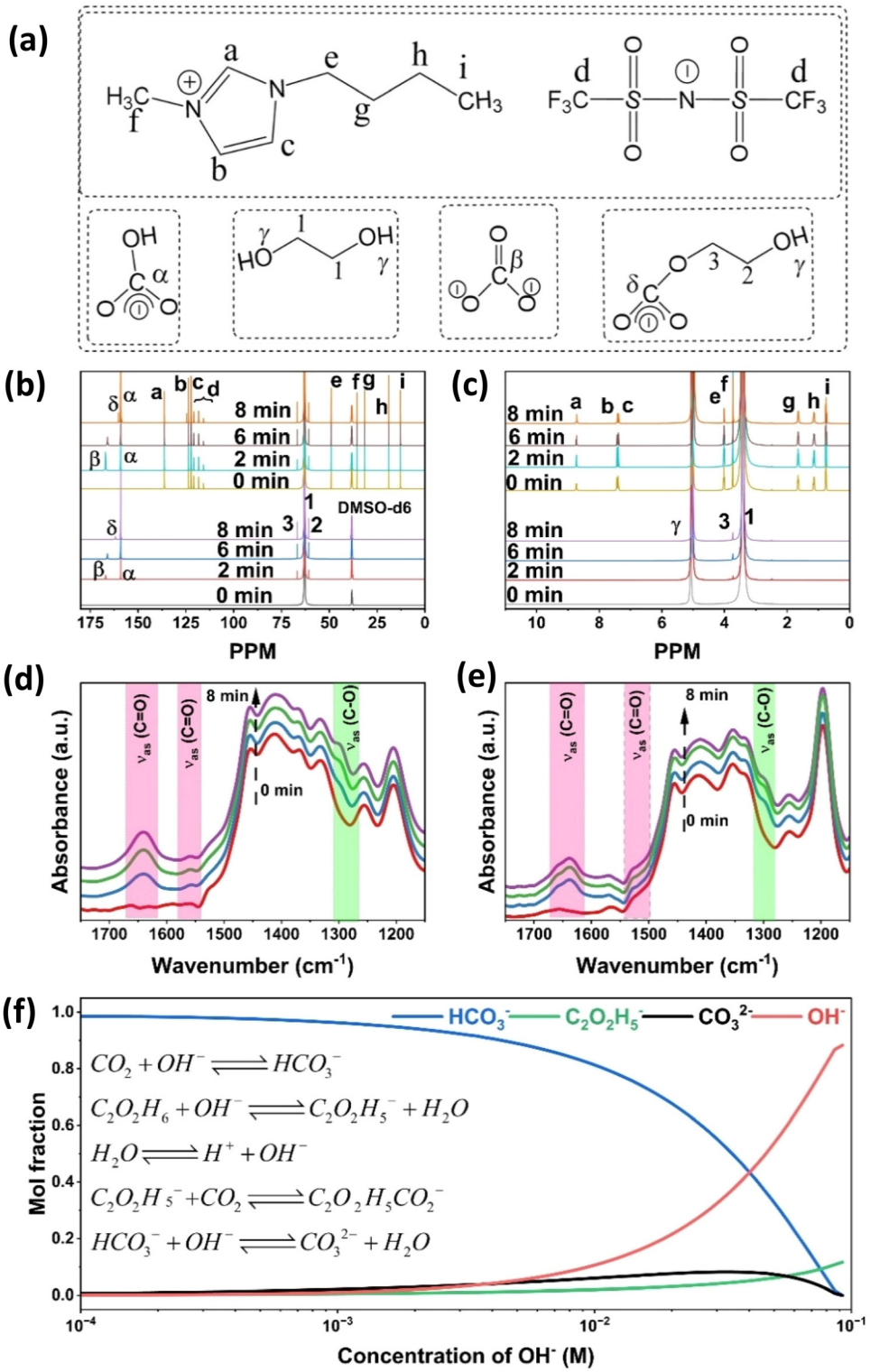

Fig. 2 (a) Chemical species observed during $^{13}CO_2$ chemisorption experiments in DES–IL mixture. (b) ^{13}C NMR spectra of $^{13}CO_2$ bubbling experiments at different time intervals with and without BMIM NTf_2, showing different species formed. (c) ^{1}H NMR spectra of $^{13}CO_2$ bubbling experiments under the same conditions. (d) IR spectra (1750–1150 cm^{-1}) of 10% CO_2 bubbling without BMIM NTf_2 at different time intervals. (e) IR spectra (1750–1150 cm^{-1}) of 10% CO_2 bubbling with BMIM NTf_2. (f) Speciation diagram of observed species as a function of OH^- concentration.

other than the formation of free bicarbonate and carbonate species.

To gain further insight, the samples were further analyzed through ^{1}H NMR, and the results are presented in Fig. 2(c).

After bubbling $^{13}CO_2$, a new peak at 3.7 ppm is observed in the system with DES. This peak is assigned to the proton associated with EG labelled as 3. A gradual shift in the peak position of –OH peaks at ~5.1 ppm can also be observed in systems containing DES and DES–IL mixtures as $^{13}CO_2$ is introduced, as shown in Fig. S3 and S4. An upfield shift in the –OH signal indicates the formation of water as a reaction product. Similar experiments were performed by Restrepo and Adams, who studied the effect of water content in glycols on ^{1}H NMR shift and outlined a technique to estimate water content in the system.[103,104]

Additional experiments were performed to confirm that CO_2 chemisorption occurred even in the presence of anhydrous flue gas (12.2% CO_2, 0.16% SO_2, 7% O_2, and 80.2% N_2). Fig. S5 and S6 show the presence of bicarbonate peaks *via* ^{13}C NMR analysis. Systems with and without BMIM NTf_2 in alkaline DES show the formation of bicarbonate. A comparison of normalized peak, at ~159 ppm, intensities also shows that even in the presence of flue gas, CO_2 chemisorption is accelerated in the system containing BMIM NTf_2, as shown in Fig. S7. Presence of water in the flue gas can have detrimental impacts on CO_2 capture process by reacting with the formed bicarbonate, yielding back to gaseous CO_2 and carbonate. Interested readers can look into already published works.[48,105] To validate the reversibility of the CO_2 chemisorption, diluted H_2SO_4 was added to the DES. Results in Fig. S8 validate our observations and prove the reversibility of CO_2 chemisorption in DES and DES–IL mixture for the pH-swing process.[48,106] Typically, for the pH swing process, the carbonate and bicarbonate species remain in equilibrium, and a basic pH preserves bicarbonate and carbonate, while an acidic pH will release CO_2 in gaseous form. The NMR shifts at 59 and 65 ppm become insignificant, indicating the reversible proton uptake by deprotonated EG and the dissolution of captured CO_2 into gaseous CO_2. Moreover, the bicarbonate peak at 159 ppm also disappears, indicating desorption of CO_2 from the system.

The DES and DES–IL systems were also simulated using quantum-chemical calculations to validate the assigned peaks from NMR experiments. Details about the simulation are also provided in Section S1. The simulated ^{13}C NMR spectra display with and without peak splitting, as shown in Fig. S9(a–c), with the corresponding chemical shift values provided in Table S2 in comparison to those of EG. This splitting of the EG peak is also observed in the experimental NMR spectra, confirming its deprotonation. Physical absorption of CO_2 is generally characterized by ^{13}C NMR signals in the range of 120–130 ppm,[107] while chemisorption results in signals mainly between 155–165 ppm. As shown in the simulated ^{13}C NMR spectrum in Figure S10(b), physisorption leads to a new carbon peak at approximately 130 ppm without any splitting of the EG peak. In contrast, chemisorption leads to a carbon peak near 163 ppm in Fig. S10(c), consistent with the experimentally observed peak at 160.9 ppm. The splitting of the EG peak in the chemisorbed state, Fig. S10(c), is assigned to EG deprotonation. The consistency between simulated and experimental data supports the conclusion that CO_2 undergoes chemisorption with DES.

Calculated NMR shifts of CO_2, bicarbonate, carbonate, and HEC are provided in Fig. S11(a)–(e) with the corresponding chemical shift values provided in Table S4. The simulated NMR spectra of deprotonated EG with CO_2, shown in Fig. S11(e), closely match the experimental peaks. This indicates the formation of a CO_2 adduct with deprotonated EG. The calculated chemical shifts at 67, 68, and 163 ppm correspond well with the experimental shifts at 61, 67, and 160.9 ppm, confirming chemisorption of CO_2 by EG. Additionally, a peak at 167 ppm in the experimental spectra, which later disappears, can be attributed to carbonate. The calculated chemical shift for carbonate appears at 184 ppm in Fig. S11(c), but may be shifted upfield due to the experimental reaction environment. This supports the experimental observation that the peaks at 159, 160.9, and 167 ppm in the ^{13}C NMR spectra correspond to bicarbonate, HEC, and carbonate species, respectively, indicating that both species are present at the onset of the reaction. The formation of a hydrogen peak at 5.9 ppm in the simulated ^{1}H NMR spectrum of water contributed to the combination of the deprotonated hydrogen from EG and the hydroxyl ion from KOH, which correlates well with the 5.1 ppm peak observed in the experimental spectra. This assignment, as illustrated in Fig. S12 with the corresponding chemical shift values provided in Table S5, confirms the presence of water in the reaction system.

Quantum calculations were also carried out for $BMIM^+$ and its interaction with CO_2, as shown in Fig. S13(a and b), with the corresponding chemical shift values provided in Table S6. The simulated ^{13}C NMR spectra for the DES–IL mixture in Fig. S13(b) reveal a new peak at around 162 ppm, as well as splitting of the C_3 and C_6 peaks upon CO_2 interaction with $BMIM^+$. However, this splitting is never observed in the experimental spectra, indicating that the $BMIM^+$ cation does not interact with CO_2. Theoretical NMR peaks for NTf_2^- and its interaction with CO_2 are also shown in Fig. S14(a–c) with the corresponding chemical shift values provided in Table S7. Similar to $BMIM^+$, if CO_2 were to interact with the NTF_2^- anion, as depicted in Fig. S13(b and c), one would expect peak shifting and the appearance of an additional carbon signal in the ^{13}C NMR spectra. Since no such peak shifting or additional peak is observed experimentally, it can be concluded that the anion does not chemically bond with CO_2. Similarly, the absence of new peaks and chemical shifts corresponding to cation–anion interactions with CO_2 in the experimental spectra suggests a plausible mechanism: BMIM NTF_2 can function as a catalyst in the absorption of CO_2 in the alkaline DES–IL system.

While promoter species are known to enhance kinetics in amine-based CO_2 capture systems, the literature also recognizes that promoters may participate directly in CO_2-binding equilibria, and promoter–CO_2 reaction products can be present under capture conditions.[108] In contrast, post-absorption NMR spectra of our system show no new peaks attributable to irreversible IL–CO_2 adduct formation or IL degradation, indicating that the ionic liquid remains chemically conserved under the studied conditions. Taken together, these observations are consistent with an IL-enabled kinetic enhancement that occurs without measurable consumption of the ionic

liquid, suggesting that the system exhibits catalytic contributions rather than solely conventional promoter behavior.

2.1.2. Experimental FTIR and quantum-chemical calculations. Fig. 2(d) represents the FTIR spectra of experiments carried out with 10% CO_2 (vol%, balance N_2) bubbling in the absence of BMIM NTf_2 in alkaline DES. New peaks are observed at 1638, 1558, 1300 cm^{-1} after 10% CO_2 is bubbled in the system. Peaks at 1635 and 1558 cm^{-1} are associated with the C═O stretching band of bicarbonate and carbonate species.[4,109,110] The shoulder peak at 1300 cm^{-1} is ascribed to the stretching band of the C–O stretching vibration of HO–CH_2–CH_2–O–COO^-. A similar band assignment was also made at 1296 cm^{-1} by Cheng *et al.* where CO_2 absorption took place in a deep eutectic solvent comprising EG.[111] Fig. 2(e) represents the FTIR spectra of 10% CO_2 (vol%, balance N_2) bubbling in the presence of BMIM NTf_2 in alkaline DES. Three new peaks are observed at 1639, 1529, and 1300 cm^{-1}, which are similar to the FTIR results obtained for the system without IL. These results also align with our previous NMR spectroscopy observations. Thus, corroborating our assumption that IL does not participate or form a chemical bond with CO_2 in the reaction and acts like a catalyst for CO_2 absorption in our system. Full spectra from the FTIR experiment with and without IL in alkaline DES have also been provided in Fig. S15 and S16. Additional information on experimental methods of FTIR is provided in Section S1.

The interaction between CO_2 and EG was further examined through simulated IR spectroscopy, as shown in Fig. S17. Comparison of the simulated IR spectra of hydroxyethyl carbonate (HEC) and EG reveals the appearance of new peaks at 1262, 1474, and 1649 cm^{-1} in the HEC spectrum. The peak at 1262 cm^{-1} in HEC closely corresponds to bands in the simulated spectra of bicarbonate (HCO_3^-) at 1278cm^{-1} and carbonate (CO_3^{2-}) at 1311 cm^{-1} and is assigned to C═O and C–O stretching vibrations. The band at 1649 cm^{-1} in HEC matches the corresponding band in HCO_3^- and is assigned to the asymmetric stretching vibration of CO_2. The peak at 1474 cm^{-1} is assigned to the symmetric stretching vibration of C═O. This band is absent in the simulated spectra of EG, HCO_3^-, and CO_3^{2-}, where the molecular symmetry remains preserved. The assigned peaks in the simulated IR spectra agree well with the experimental bands at 1300, 1558, and 1638 cm^{-1}. These results are consistent with the FTIR experimental observations, confirming the chemical interaction of CO_2 with EG and the formation of bicarbonate and carbonate species.

2.1.3. Chemical pathways and kinetic modeling. Since all the possible species during CO_2 chemisorption, in DES and DES–IL mixtures, were identified *via* NMR and FTIR, a set of equilibrium reactions was defined as shown in Section S2. These reactions were then used to monitor the dominant species as the hydroxide concentration changed during CO_2 chemisorption. Details about the dissociation constant are provided in Section S2. Fig. 2(f) and Fig. S18(a) show the speciation diagram obtained by solving the equations in Section S2.1. It can be observed that bicarbonate becomes the dominant species after ~20 mM of hydroxide has been converted. The concentration of deprotonated ethylene glycol decreases monotonically as the hydroxide concentration decreases. The speciation diagram reflects the increase and decrease of free carbonate species as observed from NMR experiments. A similar analysis was also carried out, including water in the mol fraction calculations. The speciation diagram with water formed is also provided in Fig. S18(b) and (d). Using equilibrium values from the speciation diagram can aid in calculating the extent of reaction, as shown in Fig. S18(d). Overall, a reaction pathway can be outlined as follows: when CO_2 is initially introduced into DES, its alkaline nature leads to the formation of bicarbonate and carbonate. As hydroxide concentration decreases due to consumption, the carbonate undergoes a backward reaction, forming bicarbonate and hydroxyethyl carbonate (HEC). The formation of bicarbonate is still favored till it becomes the dominant species. Furthermore, the formation of water observed by NMR can also be explained, as the extent of reaction is negative and approaches zero, as shown in Fig. S11(d).

2.2. Demonstration of the catalytic activity of ionic liquid

Section 2.1 involved determining the reaction species and reaction pathways. Section 2.2 focuses on the reaction kinetics and impact of temperature during CO_2 chemisorption in DES with and without ionic liquid. Since NMR experiments become time-intensive and expensive as the number of samples increases, an automated screening platform was employed in this study, as shown in Fig. S19. Additional information about the screening platform and the calibration is provided in Section S1. Fig. 3(a) demonstrates the enhancement of conversion rates of hydroxide with and without IL at room temperature, 298 K. To validate our analysis, we performed 5 independent measurements of conversion *versus* time with and without IL. As shown in Fig. 3(a), it is clearly evident that the enhancement of CO_2 capture rates in the presence of IL is different. Additionally, to determine if the difference is statistically significant, we performed a paired *t*-test, yielding a *t*-statistic value of −3.83, which supports the claim that the enhancement is statistically significant. Based on the analysis, the observed enhancement is statistically significant. Furthermore, when these experiments were conducted in a 3 M Hollow fiber module, similar enhancement of CO_2 hydroxylation was also observed, as shown in Fig. S20. Additional details about the hollow fiber module experiment are provided in Section S1.

Since an increased activity for CO_2 chemisorption to bicarbonate was observed, experiments were conducted at higher temperatures to determine the activation energy (E_a) and to understand the applicability in a large-scale process.[112–114] Experiments were conducted at different temperatures in a similar setup modified with a heating plate at the bottom of the glass vial to obtain E_a. Fig. 3(b) shows the comparison of the increase in reaction rates with temperature for DES without IL and with IL. Assuming a pseudo 1st order reaction is involved for the conversion of hydroxide to bicarbonate, the rate constants were determined to be 0.29, 0.43, 0.84, and 1.53 min^{-1} at 298 K, 313 K, 323 K, and 333 K, for the system without IL,

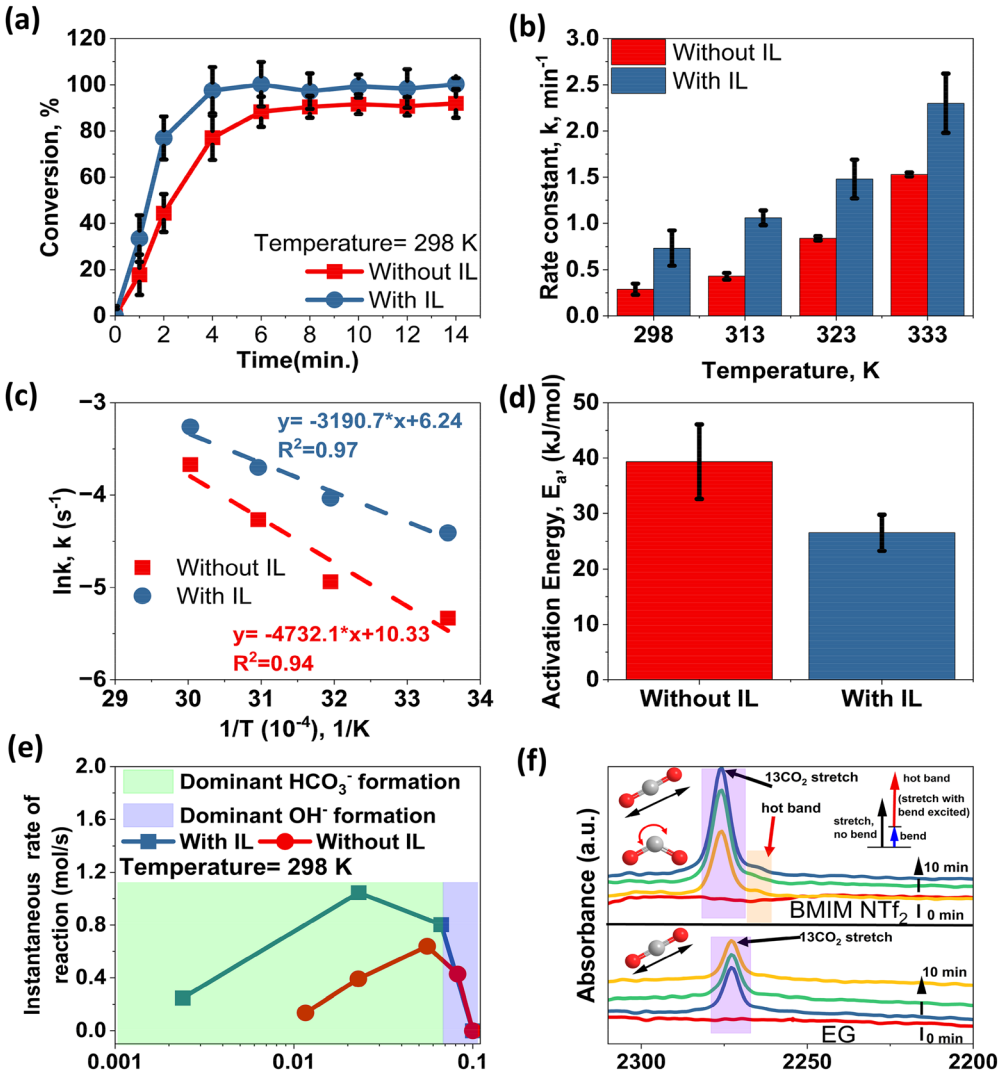

Fig. 3 (a) Time-dependent hydroxide conversion in the presence of IL and without IL. IL is BMIM NTf_2 at a mixed volume percentage of 5%. All experiments were conducted at 298 K, with an initial concentration of 0.1 M KOH to compare the influence of IL. The feed gas consists of 10% CO_2, and the balance is N_2 gas. (b) Comparison of reaction rate constants obtained by pseudo 1st order model fitting. (c) Arrhenius plots for the CO_2 capture system with and without IL. (d) Comparison of activation energies (E_a) for the CO_2 capture system with and without IL. (e) Instantaneous reaction rates *vs.* hydroxide concentration to identify the dominant reaction pathway during CO_2 chemisorption. The green region denotes predominant bicarbonate formation/dissociation, while the purple region denotes predominant water dissociation/formation. ζ_1 and ζ_3 are the extent of reaction coefficients associated with the bicarbonate and water formation. (f) FTIR spectrum of the asymmetric stretching mode of $^{13}CO_2$ at 2277 cm^{-1} in BMIM NTf_2 and at 2272 cm^{-1} in EG. The hot band absorption of the asymmetric stretch when the bend is thermally excited appears at ~2265 cm^{-1}.

respectively, as shown in Fig. 3(b) and Table S8. Furthermore, for the system containing BMIM NTf_2, the rate constants were determined to be 0.73, 1.06, 1.48, and 2.3 min^{-1} at 298 K, 313 K, 323 K, and 333 K. Additional details regarding the pseudo 1st order reaction calculations are provided in Section S1. Timed data for CO_2 hydroxylation at different temperatures are provided in Fig. S21. Furthermore, while the catalytic enhancement appears most pronounced at lower temperatures, this trend cannot be attributed to viscosity effects. A comparison of viscosity values for systems with and without IL shows a difference of only ~1 cP at room temperature, which decreases further at elevated temperatures. Thus, changes in viscosity with temperature are insufficient to explain the diminished catalytic enhancement at higher temperatures. Instead, CO_2 hydroxylation is primarily governed by the activation energy associated with CO_2 activation and solvent reorganization. As reported by Iida *et al.*[64] this barrier dominates the reaction kinetics. At higher temperatures, the intrinsic thermal energy increasingly overcomes this activation barrier even in the absence of IL, reducing the relative benefit of IL-induced solvent reorganization, making the catalytic effect less distinguishable. We also acknowledge that CO_2 solubility decreases at elevated temperatures, particularly in organic systems. However, at the compositions investigated (5 vol% IL), the measured Henry constants for EG and EG–IL mixtures are comparable[115] (~485 bar *vs.* ~415 bar), indicating only a

modest increase in CO_2 solubility upon IL addition. Such a difference corresponds to a relatively small change in dissolved CO_2 concentration and is insufficient to account for the observed enhancement in capture rate. Therefore, while solubility effects may contribute to the overall behavior, they cannot alone account for the magnitude of the kinetic enhancement observed in the DES–IL system.

Fig. 3(c) shows the Arrhenius plot for estimating the E_a of CO_2 chemisorption in the EG/KOH and EG/KOH/BMIM NTf_2 system. Activation energy (E_a) values for CO_2 chemisorption were determined by linear regression, yielding a satisfactory fit. It is evident that systems containing IL possess a reduced E_a for CO_2 chemisorption, since the magnitude of the slope of the system containing IL is significantly lower than that of the system without IL. Fig. 3(d) shows a comparison of E_a with and without IL. The E_a required for the CO_2 hydroxylation system without IL is 39.3 kJ mol^{-1}, while the system with IL requires 26.6 kJ mol^{-1}, which is a 33% reduction in E_a for CO_2 chemisorption. Results from Eyring analysis of the same data shown in Table S9 revealed a similar drastic decrease in activation enthalpy and entropy (ΔH and ΔS), indicating that the rate constant enhancement is primarily governed by the ionic-liquid transition state. Such changes in the E_a were also observed by Hsieh *et al.*,[84] who argued that the presence of ionic liquid can assist in the development of less charge at the transition state. In other words, the presence of ionic liquid modifies the nature of the transition state, which determines the extent of bond formation/breaking involved in bicarbonate/carbonate species.

Furthermore, Wang *et al.*[116] have already argued that ILs reduce the activation barrier for CO_2 hydroxylation by stabilizing polarized CO_2 and key reaction intermediates through electrostatic interactions and hydrogen bonding. These interactions distort the linear CO_2 molecule and facilitate nucleophilic attack, lowering the energetic cost of CO_2 activation compared to non-ionic solvent environments. Another review by Wang *et al.*[117] discusses the Arrhenius analysis reported for the synthesis of dimethyl carbonate (DMC) from CO_2 and methanol in the presence of $[GLY(mim)_3][NTf_2]_3$, which demonstrates a clear reduction in the apparent activation energy relative to the IL-free system. This decrease is attributed to strong electrostatic interactions and hydrogen bonding between the ionic liquid and CO_2, which stabilize activated CO_2 species and key transition states. The ionic liquid also enhances local reactant organization and polarizes CO_2, thereby lowering the energetic cost of bond rearrangement. Collectively, these effects accelerate reaction kinetics, confirming the role of ionic liquids as catalysts. To validate, the enhancement in capture rate also occurs in the presence of IL under DAC-relevant conditions. We performed an additional experiment, details of which are provided in Section S1. As shown in Fig. S22, under 500 ppm CO_2 feed conditions, the CO_2 conversion rate is also enhanced by the presence of IL. The kinetics under 500 ppm CO_2 conditions are sluggish due to a decrease in the effective driving force.[118,119]

Since it is evident that CO_2 chemisorption is catalyzed, the next step is to identify the reaction catalyzed by the IL. To investigate this, the instantaneous reaction rates *vs.* concentration of OH^- are plotted in Fig. 3(e). By comparison with the magnitude of the extent of the reaction as shown in Fig. S23, it can be further confirmed that reaction 1, *i.e.*, bicarbonate formation, is catalyzed, as shown in the green region, since the maximum instantaneous reaction rate overlaps with the bicarbonate formation region. Furthermore, ζ_1 (extent of reaction 1) becomes dominant after ~25% conversion of hydroxide has taken place, as shown in Fig. 3(e) and Fig. S23. As previously discussed, the presence of IL lowers the activation energy for bicarbonate formation by bending CO_2. Additionally, in Fig. S23 and S18(d), the ζ_3 (extent of reaction 3) dominated region is small and negative, indicating that water formation occurs in this region during the initial time steps of CO_2 bubbling. This is further validated by the significant NMR upfield shifts observed in OH^- peaks at ~5.1 ppm only at the initial time steps of CO_2 bubbling, in Fig. S3 and S4.

Based on the extent-of-reaction analysis, the bicarbonate formation pathway is clearly catalyzed. As discussed in the Introduction, facilitated CO_2 bending can lower the effective activation barrier, thereby catalyzing CO_2 hydroxylation to bicarbonate.[64] To experimentally probe whether enhanced CO_2 bending occurs in the ionic liquid (IL) environment, ATR-FTIR spectroscopy was employed. The bending mode of $^{12}CO_2$ (~660 cm^{-1}) lies at sufficiently low frequency that, at room temperature ($k_BT \approx 200$ cm^{-1}), it is thermally populated for a small but non-negligible fraction of CO_2 molecules.[58,120] To eliminate interference from atmospheric CO_2, isotopically labeled $^{13}CO_2$ was used. As shown in Fig. 3(f), $^{13}CO_2$ exhibits an asymmetric stretching band at 2277 cm^{-1}. In the presence of BMIM NTf_2, the intensity of this band increases with time, accompanied by the emergence of a weak shoulder approximately 11 cm^{-1} lower in frequency. This shoulder has been previously assigned to a hot band arising from coupling between the thermally populated bending mode and the asymmetric stretch, leading to an apparent red shift of the absorption feature.[61,63] In contrast, for EG, no hot band is observed even after 10 minutes of $^{13}CO_2$ bubbling, and the intensity of the $^{13}CO_2$ asymmetric stretch at ~2272 cm^{-1} remains unchanged. In ionic liquids, strong and spatially heterogeneous local electric field gradients disrupt the symmetric solvation shell around CO_2, increasing polarization and enhancing the population of thermally accessible bent vibrational states. This manifests as increased coupling between the bending and asymmetric stretch modes, without requiring direct chemical coordination of CO_2 to the ions.[63] These observations indicate that enhanced CO_2 bending occurs selectively in the presence of the IL, supporting our conclusion that the IL environment facilitates CO_2 activation and thereby catalyzes bicarbonate formation.

Several alternative explanations could, in principle, be invoked to rationalize the observed enhancement in CO_2 hydroxylation rates in the presence of ionic liquids (ILs). (a) CO_2 solubility effects. BMIM NTf_2 is indeed known for its high intrinsic CO_2 solubility; however, the IL loading employed in

this study is limited to 5 vol%, corresponding to a mol fraction of ~0.05. At this low concentration, recent calculations from our group show that the Henry's constant (k_H) decreases only modestly (from ~500 bar to ~270 bar), compared to the value for pure IL (~29 bar).[115,121,122] This relatively small change in k_H cannot account for the drastic enhancement in hydroxylation rates observed, ruling out solubility-driven effects as the dominant mechanism. (b) Viscosity effects. The viscosity of pure BMIM NTf_2 (~48 cP) is higher than that of ethylene glycol (~22 cP); however, applying a logarithmic mixing rule yields an estimated viscosity of ~23 cP at a 0.05 mol fraction of IL, which is an increase of only ~1 cP. Such a marginal change would be expected to slightly *impede*, rather than accelerate reaction kinetics, further weakening viscosity as a plausible explanation. (c) Mass-transfer limitations. All experiments were performed under conditions designed to ensure kinetic control. As shown in Fig. S24, increasing the CO_2 flow rate beyond 10 mL min^{-1} does not further enhance hydroxylation rates, indicating saturation of the gas–liquid mass transfer rates. This behavior confirms that the system operates in a kinetically limited regime rather than being governed by external mass-transfer constraints. (d) Interfacial effects. While IL cations with long alkyl chains are known to be surface-active and may accumulate at the gas–liquid interface, this interfacial structuring does not explain the observed rate enhancement. In fact, as demonstrated in the subsequent section, increasing the IL concentration beyond an optimal value leads to slower CO_2 hydroxylation, consistent with interfacial saturation and mass-transfer hindrance rather than acceleration. Taken together, these analyses demonstrate that changes in CO_2 solubility, viscosity, mass transfer, or interfacial effects cannot rationalize the experimentally observed rate enhancement. Thus, the only explanation consistent with all observations is that the IL plays a catalytic role in facilitating CO_2 hydroxylation.

2.3. Mechanism of ionic liquid-catalyzed CO_2 capture

To explore the impact of concentration, *i.e.*, volume% of ILs in the EG/KOH system, additional experiments were also conducted at 10 vol% and 20 vol%, respectively. Fig. 4(a) shows the CO_2 chemisorption kinetics at 5 vol%, 10 vol%, and 20 vol% of BMIM NTf_2 in the DES–IL system. The BMIM NTf_2 system could achieve 50% conversion at 1.6 min, 2.8 min, and 5 min for 5 vol%, 10 vol%, and 20 vol%, respectively. Correspondingly, the pseudo-1st-order rate constants were 0.6, 0.24, and 0.15 min^{-1} for 5 vol%, 10 vol%, and 20 vol%, respectively, of BMIM NTf_2, as shown in Table S8. Additional experiments were also conducted with 1-hexyl-3-methyl-imidazolium bis(trifluorosulfonyl)imide (HMIM NTf_2), as shown in Fig. 4(b), and the corresponding rate constants are also provided in Table S8. A similar trend was also observed in HMIM NTf_2 when BMIM NTf_2 was replaced in the DES–IL mixture. In summary, the chemisorption kinetics decline with increasing IL concentration. This behavior is unlikely due to the catalytic role of ILs, as higher concentrations would typically enhance reaction rates.[123,124] Instead, the decline in reaction rates is more likely attributed to interfacial effects, specifically, the decline in interfacial area of the DES–IL solution, which can hinder gas–liquid mass transfer.[125–128]

To elucidate the impact of the interfacial area of the fluid on CO_2 chemisorption phenomena, a mathematical model based on mass transfer in a bubble column was developed to describe the underlying reaction mechanisms and changes in interfacial property.[129–131] Inspired by the Michaelis–Menten kinetics,[132,133] the mathematical model approximates the reaction of IL with CO_2 as a pseudo-steady state reaction, as shown in eqn (1), where the IL acts as a catalytic site that transiently binds CO_2 to form an intermediate complex. After $ILCO_2$ is formed, the reaction proceeds with the hydroxide dissolved in the liquid as shown in eqn (2). The rate law model, combined with the bubble column mass transfer model, was then fit to a system containing different volume percentages of IL, using experimental data on CO_2 chemisorption with a DES–IL mixture to gain insight into the model parameters. Such an approach captures the saturation behavior observed at higher IL concentrations, where mass transfer or subsequent reaction steps, rather than CO_2 binding, become rate-limiting.

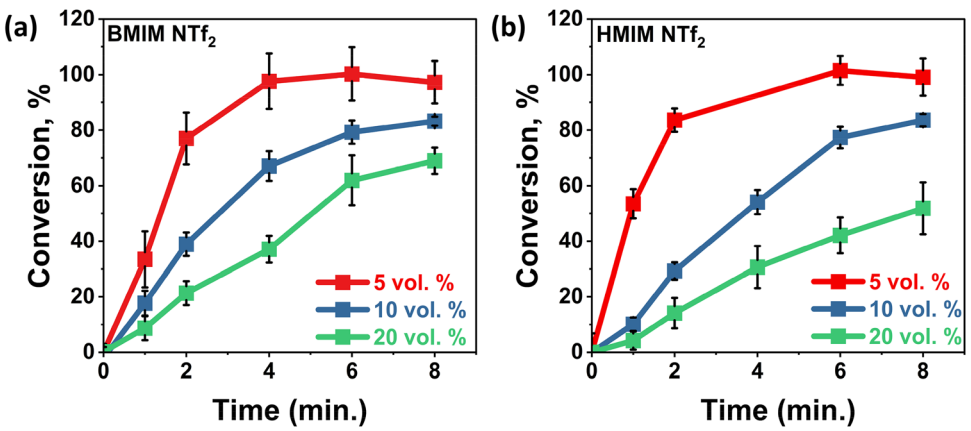

Fig. 4 Time-dependent hydroxide conversion at varying volume percentages of (a) BMIM NTf_2 and (b) HMIM NTf_2. All experiments were conducted at 298 K, and an initial concentration of 0.1 M KOH was used to compare the influence of varying volume percentage of IL.

Additional details about the mathematical model, reactions, and assumptions are provided in Section S3.

$$IL + CO_2(l) \underset{k_{-1}}{\overset{k_1}{\rightleftharpoons}} ILCO_2 \quad (1)$$

$$ILCO_2 + OH^- \xrightarrow{k_2} ILHCO_3^- \quad (2)$$

Results from model fitting are in satisfactory agreement, as shown in Fig. S26. Importantly, the interfacial surface area of the bubbles was found to decrease as the volume percentage of IL increased. This is counterintuitive since the surface tension of bubbles decreases as the concentration of IL increases. The decline in interfacial surface area is likely caused by saturation of the liquid surface with IL molecules. At high IL concentrations, the CO_2–IL interactions likely dominate, thereby reducing the interactions of CO_2 with the OH^- ions and ultimately slowing the chemisorption process. Similar behavior was also observed when BMIM NTf_2 was replaced with HMIM NTf_2, and the fitting results are provided in Fig. S27 and Table S10. This effect can be rationalized by the findings of Mezger *et al.*[134] who reported that high IL concentrations lead to layering of alternate cations and anion-enriched regions at the liquid interface. Such layers can often decrease mass transfer coefficients and ultimately impact the diffusion coefficients of gas molecules.[135]

2.4. Impact of different cations and anions on CO_2 chemisorption

To explore the impact of cations and anions of ILs, additional experiments were conducted with a 5 volume% IL as discussed in Section S1. The list of ILs screened in this work is shown in Table S1. Fig. 5(a) shows the data obtained for EMIM NTf_2 in DES. Clearly, the reaction rates are significantly higher than those of the IL as compared to those without IL. The EMIM-based IL system could achieve 50% conversion at 1.7 min and 1.9 min for EMIM OTf and EMIM NTf_2. For EMIM-based ILs, the rate constants obtained in Fig. S25 are almost constant and follow the order: OTf ≈ NTf_2 > No IL.

Fig. 5(b) shows the chemical conversion of KOH in the presence of BMIM-based ILs. Almost all BMIM-based ILs show enhanced CO_2 chemisorption kinetics. The BMIM-based IL system could achieve 50% conversion at 0.68 min, 0.95 min, 1.6 min, and 2.8 min for BMIM OTf, BMIM I, BMIM DCA, BMIM NTf_2, and BMIM PF6. For BMIM-based ILs, the rate constants are shown in Fig. S25 and follow the decreasing trend: I > OTf > DCA > NTf_2 > PF6.

Fig. 5(c) shows the chemical conversion of KOH in the presence of HMIM-based ILs. Similarly, all HMIM-based ILs show enhanced CO_2 chemisorption kinetics compared to chemisorption in alkaline DES alone. The HMIM-based IL system achieved 50% conversion at 0.94 min, 1.3 min, and 1.4 min for HMIM PF_6, HMIM I, HMIM OTf, and HMIM NTf_2, respectively. For HMIM-based ILs, the rate constant follows almost the same order as what has been observed before. The 1st-order rate constants follow the order HMIM OTf > HMIM NTf_2 > HMIM I > HMIM PF_6, as shown in Fig. S28. When compared with a fixed cation such as NTf_2 and a varying cation, the 1st order rate constants follow a general order: EMIM > BMIM > HMIM, as observed in Table S8. Overall, the current study revealed that the nature of anion and cation also plays an important role in the enhancement of CO_2 chemisorption rates. Furthermore, the choice of anion seems to become less significant towards the improvement of CO_2 capture kinetics in ILs with cations with longer alkyl chain substitutions.

Although the scope of the present study does not include a comprehensive techno-economic analysis (TEA), detailed kinetic modeling, or process-scale simulations for DES–IL systems, if future studies establish process feasibility, the use of volume percentages may be practically relevant at an industrial scale. However, differences in rate enhancement arising from various anions and cations may also reflect differences in molar loading. To account for this, we performed experiments under equimolar conditions, maintaining a fixed ionic liquid concentration of 0.1 M and a 0.1 M hydroxide concentration in the DES capture solution. As shown in Fig. S29, DCA^- anion-based ILs consistently exhibit slightly slower kinetics compared

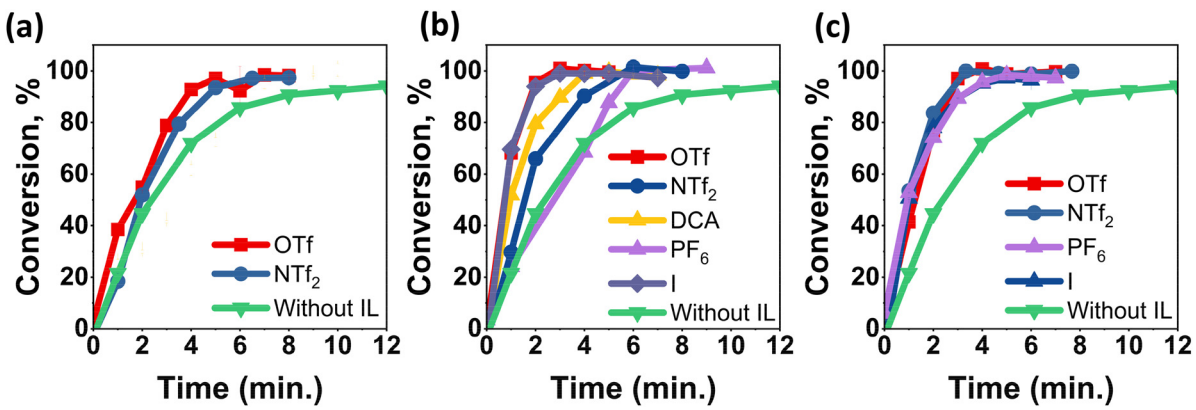

Fig. 5 Time-dependent hydroxide conversion in the presence of (a) EMIM-based ILs, (b) BMIM-based ILs, and (c) HMIM-based ILs. All experiments were conducted at 298 K, 5 volume percentage IL, and an initial concentration of 0.1 M KOH to compare the influence of IL cation and anion structure on conversion rates.

to OTf^- and NTf_2^- based ILs, although they still provide measurable enhancement in CO_2 hydroxylation relative to the IL-free system.

Based on Fig. S29, one might argue that at equimolar IL concentrations, CO_2 solubility governs the observed enhancement. This interpretation is reasonable for DCA^- based ILs, which are known to exhibit lower CO_2 solubility and correspondingly reduced enhancement relative to OTf^- and NTf_2^- based ILs.[136,137] However, distinguishing between OTf^- and NTf_2^- anions based solely on CO_2 solubility becomes less straightforward. For EMIM-based ILs, NTf_2^- shows significant enhancement over OTf^-, whereas for HMIM-based ILs, OTf^- outperforms NTf_2^-. In contrast, BMIM-based ILs exhibit comparable performance for both OTf^- and NTf_2^- anions. These trends suggest that CO_2 solubility alone cannot consistently explain the observed rate enhancements across different cation–anion combinations.

Another possible explanation is viscosity effects. However, accounting for viscosity also does not support the observation in Fig. S29. For example, BMIM DCA, which has the least viscosity of approximately 28 cP, exhibits the least enhancement among the ILs studied. Interestingly, although the viscosity of BMIM OTf is roughly twice that of BMIM NTf_2^-, both ILs display similar enhancement in CO_2 hydroxylation rates. While some differences are observed between $EMIM^+$ and $HMIM^+$ cation based-ILs, there is no systematic correlation between viscosity and rate enhancement. Therefore, the argument that viscosity tracks with the enhancement observed in these experiments is not supported by the data.

Collectively, these results indicate that the observed rate enhancement cannot be attributed solely to CO_2 solubility or viscosity effects. Instead, we emphasize that the enhancement arises from a combination of catalytic, interfacial, electrostatic, and solubility effects introduced by ILs. A more detailed molecular-level investigation, potentially involving DFT or molecular mechanics simulations of the gas–liquid interfacial structure, would be required to fully deconvolute these contributions, but such an analysis lies beyond the scope of the present work.

3. Conclusions

In this work, we presented a mechanistic understanding of IL-based alkaline DES mixtures for enhancing CO_2 capture rates. ^{13}C, ^1H NMR, and FTIR analysis assisted in elucidating the reaction species and mechanisms, revealing the formation of carbonates, water, and bicarbonate during CO_2 chemisorption. The process begins with CO_2 hydroxylation, producing bicarbonates, carbonates, and water. As hydroxide is consumed, the carbonates undergo a backward reaction to form bicarbonate, consistent with the Henderson–Hasselbalch equation, ultimately leading to bicarbonate as the dominant species in the solution for the CO_2 absorption experiment. Performing Arrhenius and Eyring analyses, we observed that the optimal IL concentration modulates the activation enthalpy and entropy, thereby reducing the activation barrier for CO_2 hydroxylation. Additional experiments under DAC-relevant conditions also demonstrate IL's catalytic activity for CO_2 hydroxylation. Using ATR-FTIR, we also observed CO_2 bending by identifying hot bands in IL. This validates the idea that IL enhances CO_2 bending, which in turn modifies the solvent reorganization around CO_2, thereby catalyzing the formation of bicarbonate. Reaction in the presence of IL-based alkaline mixtures can be described by a Michaelis–Menten-type model, in which the IL acts as a catalytic site that transiently binds CO_2 to form an intermediate complex. Furthermore, the work highlights the importance of solution properties, such as the surface tension of IL-based alkaline DES mixtures, which can impact the mass transfer coefficient during CO_2 capture. Finally, the roles of anions and cations were also elucidated, highlighting the contributions of each species to the CO_2 chemisorption process. Collectively, these results indicate that the observed rate enhancement cannot be attributed solely to CO_2 solubility or viscosity effects. Instead, we emphasize that the enhancement arises from a combination of catalytic, interfacial, electrostatic, and solubility effects introduced by the presence of ILs. Such analyses will help tailor the individual components of the DES–IL mixture and may inform the design of systems to improve CO_2 capture performance, including under low-concentration conditions relevant to direct air capture.

Conflicts of interest

There are no conflicts to declare.

Data availability

The data supporting this article have been included as part of the supplementary information (SI). Supplementary information is available. See DOI: https://doi.org/10.1039/d6ey00026f.

Acknowledgements

This material is based on the work performed in the Materials and Systems Engineering Laboratory at the University of Illinois Chicago in collaboration with Dr Jindal Shah's Lab. This material is based upon work supported by the U.S. Department of Energy, Office of Science, Office of Basic Energy Sciences Direct Air Capture program under Award Number DE-SC-0022321. M. R. S. acknowledges funding support from the U.S. National Science Foundation – ECO-CBET program (award no. 2420733).

References

1 K. Raja, *Barriers and opportunities in achieving washington state's target of a 100 percent clean energy grid by 2045*, 2024, pp. 1–57.
2 C. N. S. Summit, Carbon Capture. CARBON 2022.

3 A. D'Souza, K. Hoyt, C. M. Snyder and A. Stapp, *Can Operation Warp Speed Serve as a Model for Accelerating Innovations Beyond Covid Vaccines?*, National Bureau of Economic Research, 2024.
4 S. Meng, T. Lambert and P. Milner, Harnessing Oxidized Amines as Robust Sorbents for Carbon Capture, *J. Am. Chem. Soc.*, 2024, **147**, 6786–6794.
5 W. Ampomah, A. Morgan, D. O. Koranteng and W. I. Nyamekye, CCUS Perspectives: Assessing Historical Contexts, Current Realities, and Future Prospects, *Energies*, 2024, **17**(17), 4248.
6 J. Ma, L. Li, H. Wang, Y. Du, J. Ma, X. Zhang and Z. Wang, Carbon capture and storage: history and the road ahead, *Engineering*, 2022, **14**, 33–43.
7 J. L. Míguez, J. Porteiro, R. Pérez-Orozco, D. Patiño and S. Rodríguez, Evolution of CO2 capture technology between 2007 and 2017 through the study of patent activity, *Appl. Energy*, 2018, **211**, 1282–1296.
8 R. R. Wanderley, D. D. Pinto and H. K. Knuutila, From hybrid solvents to water-lean solvents–A critical and historical review, *Sep. Purif. Technol.*, 2021, **260**, 118193.
9 E. Hunter-Sellars, J. D. Kerr, H. V. Eshelman, Z. A. Pollard, A. J. Varni, M. A. Sakwa-Novak, M. A. Marple and S. H. Pang, Oxidation of Supported Amines for CO2 Direct Air Capture: Assessing Impact on Physical Properties and Mobility via NMR Relaxometry, *Macromol. Chem. Phys.*, 2024, **225**(14), 2400023.
10 Q. Li, T. Qu, S. Tan, T. Wang, Y. Ding, C. Wang, J. Zhang, Z. Xiong and Y. Zhao, Structure–activity relationship of a dual-function amine-based electrolyte for integrated CO2 capture and electrochemical conversion, *Chem. Eng. J.*, 2024, **498**, 155056.
11 Y.-F. Ren, B.-H. Chen, X.-Y. Chen, H.-W. Du, Y.-L. Li and W. Shu, Direct synthesis of branched amines enabled by dual-catalyzed allylic C–H amination of alkenes with amines, *Sci. Adv.*, 2024, **10**(14), eadn1272.
12 F. Shadab, I. I. Alkhatib and L. F. Vega, Guiding the Selection of Novel Amines for CO2 Capture Using a Molecular-Based and Multicriteria Modeling Approach, *Energy Fuels*, 2024, **38**(18), 17805–17821.
13 X. Y. D. Soo, J. J. C. Lee, W.-Y. Wu, L. Tao, C. Wang, Q. Zhu and J. Bu, Advancements in CO2 capture by absorption and adsorption: A comprehensive review, *J. CO2 Util.*, 2024, **81**, 102727.
14 V. D. Ola, M. E. Mohyaldinn, T. O. Olugbade and A. H. Amadi, Corrosion in Amine Gas Capturing Facilities: Processes, Challenges, and Mitigations—a Review, *Process Integr. Optim. Sustain.*, 2024, 1–28.
15 N. Yotapan, N. Sriplai, S. Ruengsangtongkul and K. Sombatmankhong, Imidazoline As a Volatile Corrosion Inhibitor for Mitigation of Top-and Bottom-of-the-Line CO2 Corrosion in Carbon Steel Pipelines, *Langmuir*, 2024, **40**, 11888–11902.
16 D. G. Ramlan, N. B. Juli, T. Pojtanabuntoeng and N. Yaakob, Benzylamine as Volatile Corrosion Inhibitor for Top-of-the-Line Corrosion in Water-Hydrocarbon Co-Condensation Environment, *J. Pipeline Sci. Eng.*, 2024, 100253.
17 L. Al-Mahbobi, A. Klemm, C. Taylor, B. Gurkan and E. Pentzer, CO2 Capture with Capsules of Ionic Liquid/Amines, *ACS Appl. Eng. Mater.*, 2024, **2**(5), 1298–1305.
18 C. Bettenhausen, The life-or-death race to improve carbon capture, *Chem. Eng. News*, 2021, **99**(26), 28–35.
19 C. W. Jones, CO2 capture from dilute gases as a component of modern global carbon management, *Annu. Rev. Chem. Biomol. Eng.*, 2011, **2**(1), 31–52.
20 N. Mac Dowell, P. S. Fennell, N. Shah and G. C. Maitland, The role of CO2 capture and utilization in mitigating climate change, *Nat. Clim. Change*, 2017, **7**(4), 243–249.
21 K. H. Smith, H. E. Ashkanani, B. I. Morsi and N. S. Siefert, Physical solvents and techno-economic analysis for pre-combustion CO2 capture: A review, *Int. J. Greenhouse Gas Control*, 2022, **118**, 103694.
22 L. E. Adkin, Technology innovation as a response to climate change: The case of the climate change emissions management corporation of alberta, *Rev. Policy Res.*, 2019, **36**(5), 603–634.
23 A. Read, *Climate change policy in Alberta*; Pembina Institute Calgary, 2014.
24 S. Bonham and I. Chrysostomidis Regulatory Challenges and Key Lessons Learned from Real World Development of CCS Projects. CO2 Capture Project, Final Report. https://www.co2captureproject.org/reports/regulatory_study.pdf (accessed 31 May 2016) 2012.
25 M. Ali, T. Sarwar, N. M. Mubarak, R. R. Karri, L. Ghalib, A. Bibi and S. A. Mazari, Prediction of CO2 solubility in Ionic liquids for CO2 capture using deep learning models, *Sci. Rep.*, 2024, **14**(1), 14730.
26 J. Ma, Y. Du, M. Liu, Y. Zhou, X. Wang, B. Wang, J. Zhu and M. Zhu, Design and Synthesis of Novel Dual-Functional Protic Ionic Liquids with a Superior High CO2 Absorption Efficiency, *J. Phys. Chem. B*, 2024, **129**, 372–384.
27 A. Puga, M. Yousefe, K. Glińska, R. Garcia-Valls and M. Giamberini, Hydrated carboxylate ionic liquids as chemical CO2 sorbents of high capacity and moderate enthalpy of absorption, *Sep. Purif. Technol.*, 2025, **354**, 128443.
28 N. Zhang, Z. Huang, H. Zhang, J. Ma, B. Jiang and L. Zhang, Highly efficient and reversible CO2 capture by task-specific deep eutectic solvents, *Ind. Eng. Chem. Res.*, 2019, **58**(29), 13321–13329.
29 A. J. Greer, J. Jacquemin and C. Hardacre, Industrial applications of ionic liquids, *Molecules*, 2020, **25**(21), 5207.
30 K. Lovato, P. S. Fier and K. M. Maloney, The application of modern reactions in large-scale synthesis, *Nat. Rev. Chem.*, 2021, **5**(8), 546–563.
31 C.-Z. Liu, F. Wang, A. R. Stiles and C. Guo, Ionic liquids for biofuel production: opportunities and challenges, *Appl. Energy*, 2012, **92**, 406–414.
32 F. Li, Y. Bai, S. Zeng, X. Liang, H. Wang, F. Huo and X. Zhang, Protic ionic liquids with low viscosity for

efficient and reversible capture of carbon dioxide, *Int. J. Greenhouse Gas Control*, 2019, **90**, 102801.

33 B. Gurkan, B. Goodrich, E. Mindrup, L. Ficke, M. Massel, S. Seo, T. Senftle, H. Wu, M. Glaser and J. Shah, Molecular design of high capacity, low viscosity, chemically tunable ionic liquids for CO2 capture, *J. Phys. Chem. Lett.*, 2010, **1**(24), 3494–3499.

34 A. N. Keller, P. J. Thacker, M. Baldea, M. A. Stadtherr and J. F. Brennecke, Reaction thermochemistry for carbon dioxide absorption by aprotic N-heterocyclic anion ionic liquids, *ACS Sustain. Chem. Eng.*, 2024, **12**(36), 13634–13644.

35 S. Seo, M. Quiroz-Guzman, M. A. DeSilva, T. B. Lee, Y. Huang, B. F. Goodrich, W. F. Schneider and J. F. Brennecke, Chemically tunable ionic liquids with aprotic heterocyclic anion (AHA) for CO2 capture, *J. Phys. Chem. B*, 2014, **118**(21), 5740–5751.

36 Y.-Y. Lee, D. Penley, A. Klemm, W. Dean and B. Gurkan, Deep eutectic solvent formed by imidazolium cyanopyrrolide and ethylene glycol for reactive CO2 separations, *ACS Sustain. Chem. Eng.*, 2021, **9**(3), 1090–1098.

37 Y. A. Elhamarnah, M. Nasser, H. Qiblawey, A. Benamor, M. Atilhan and S. Aparicio, A comprehensive review on the rheological behavior of imidazolium based ionic liquids and natural deep eutectic solvents, *J. Mol. Liq.*, 2019, **277**, 932–958.

38 L. Hu, L. Chen, Y. Fang, A. Wang, C. Chen and Z. Yan, Facile synthesis of zeolitic imidazolate framework-8 (ZIF-8) by forming imidazole-based deep eutectic solvent, *Microporous Mesoporous Mater.*, 2018, **268**, 207–215.

39 B. Kudłak, K. Owczarek and J. Namieśnik, Selected issues related to the toxicity of ionic liquids and deep eutectic solvents—a review, *Environ. Sci. Pollut. Res.*, 2015, **22**, 11975–11992.

40 P. D. de María and Z. Maugeri, Ionic liquids in biotransformations: from proof-of-concept to emerging deep-eutectic-solvents, *Curr. Opin. Chem. Biol.*, 2011, **15**(2), 220–225.

41 H. Vanda, Y. Dai, E. G. Wilson, R. Verpoorte and Y. H. Choi, Green solvents from ionic liquids and deep eutectic solvents to natural deep eutectic solvents, *C. R. Chim*, 2018, **21**(6), 628–638.

42 B. A. Pandey and S. Pandey, Superbase-Added Choline Chloride-Based Deep Eutectic Solvents for CO2 Capture and Sequestration, *ChemistrySelect*, 2017, **2**(35), 11422–11430.

43 B. Jiang, J. Ma, N. Yang, Z. Huang, N. Zhang, X. Tantai, Y. Sun and L. Zhang, Superbase/acylamido-based deep eutectic solvents for multiple-site efficient CO2 absorption, *Energy Fuels*, 2019, **33**(8), 7569–7577.

44 L. L. Sze, S. Pandey, S. Ravula, S. Pandey, H. Zhao, G. A. Baker and S. N. Baker, Ternary deep eutectic solvents tasked for carbon dioxide capture, *ACS Sustain. Chem. Eng.*, 2014, **2**(9), 2117–2123.

45 A. Prajapati, R. Sartape, M. T. Galante, J. Xie, S. L. Leung, I. Bessa, M. H. Andrade, R. T. Somich, M. V. Rebouças and G. T. Hutras, Fully-integrated electrochemical system that captures CO 2 from flue gas to produce value-added chemicals at ambient conditions, *Energy Environ. Sci.*, 2022, **15**(12), 5105–5117.

46 A. Prajapati, N. C. Kani, J. A. Gauthier, R. Sartape, J. Xie, I. Bessa, M. T. Galante, S. L. Leung, M. H. Andrade and R. T. Somich, CO2-free high-purity ethylene from electroreduction of CO2 with 4% solar-to-ethylene and 10% solar-to-carbon efficiencies, *Cell Rep. Phys. Sci.*, 2022, **3**(9), 1–17.

47 R. Sartape, A. Prajapati, N. C. Kani, T. Rojas, N. K. Dandu, P. Dhakal, A. S. Thorat, J. Xie, I. Bessa and M. T. Galante, Reply to the 'Comment on ''Migration-assisted, moisture gradient process for ultrafast, continuous CO 2 capture from dilute sources at ambient conditions, *Energy Environ. Sci.*, 2022, **15**(9), 3994–3996, DOI: 10.1039/D2EE00555G.

48 A. Prajapati, R. Sartape, T. Rojas, N. K. Dandu, P. Dhakal, A. S. Thorat, J. Xie, I. Bessa, M. T. Galante and M. H. Andrade, Migration-assisted, moisture gradient process for ultrafast, continuous CO 2 capture from dilute sources at ambient conditions, *Energy Environ. Sci.*, 2022, **15**(2), 680–692.

49 A. Thorat, R. Chauhan, R. Sartape, M. R. Singh and J. K. Shah, Effect of K+ force fields on ionic conductivity and charge dynamics of KOH in ethylene glycol, *J. Phys. Chem. B*, 2024, **128**(15), 3707–3719.

50 R. Mishra, R. Bhawnani, R. Sartape, R. Chauhan, A. S. Thorat, M. R. Singh and J. K. Shah, Role of intermolecular interactions in Deep Eutectic solvents for CO2 capture: Vibrational spectroscopy and quantum chemical studies, *J. Phys. Chem. B*, 2024, **128**, 10214–10229.

51 R. Chauhan, R. Sartape, R. Mishra, J. K. Shah and M. R. Singh, High-throughput measurements of CO2 permeance and solubility in ionic liquid reveal a synergistic role of ionic interactions and void fractions, *Chem. Eng. J.*, 2024, **496**, 153697.

52 A. Thorat, A. K. Verma, R. Chauhan, R. Sartape, M. R. Singh and J. K. Shah, Identifying High Ionic Conductivity Compositions of Ionic Liquid Electrolytes Using Features of the Solvation Environment, *J. Chem. Theory Comput.*, 2025, **21**, 1929–1940.

53 A. Thorat, A. K. Verma, R. Chauhan, R. Sartape, M. R. Singh and J. K. Shah, Identifying High Ionic Conductivity Compositions of Ionic Liquid Electrolytes Using Features of the Solvation Environment, *J. Chem. Theory Comput.*, 2025, **21**(4), 1929–1940.

54 R. Chauhan, R. Sartape, A. Thorat, J. K. Shah and M. R. Singh, Theory-enabled high-throughput screening of ion dissociation explains conductivity enhancements in diluted ionic liquid mixtures, *ACS Sustain. Chem. Eng.*, 2023, **11**(41), 14932–14946.

55 A. K. Verma, A. S. Thorat and J. K. Shah, Predicting Ionic Conductivity of Imidazolium-Based Ionic Liquid Mixtures Using Quantum-Mechanically Derived Partial Charges in the Condensed Phase, *J. Phys. Chem. B*, 2025, **129**(9), 2546–2559.

56 H. Li, J. Zhao, L. Luo, J. Du and J. Zeng, Symmetry-breaking sites for activating linear carbon dioxide molecules, *Acc. Chem. Res.*, 2021, **54**(6), 1454–1464.
57 X.-D. Lang, X. He, Z.-M. Li and L.-N. He, New routes for CO2 activation and subsequent conversion, *Curr. Opin. Green Sustain. Chem.*, 2017, **7**, 31–38.
58 C. H. Giammanco, P. L. Kramer, S. A. Yamada, J. Nishida, A. Tamimi and M. D. Fayer, Coupling of carbon dioxide stretch and bend vibrations reveals thermal population dynamics in an ionic liquid, *J. Phys. Chem. B*, 2016, **120**(3), 549–556.
59 M. Qiu, J. Li, H. Wu, Y. Huang, H. Guo, D. Gao, L. Shi and Q. Yi, One-pot non-covalent heterogenization and aromatization of poly (ionic liquids) for metal-/cocatalyst-free and atmospheric CO2 conversion, *Appl. Catal., B*, 2023, **322**, 122125.
60 J. A. Schott, C.-L. Do-Thanh, W. Shan, N. G. Puskar, S. Dai and S. M. Mahurin, FTIR investigation of the interfacial properties and mechanisms of CO2 sorption in porous ionic liquids, *Green Chem. Eng.*, 2021, **2**(4), 392–401.
61 T. Brinzer, C. A. Daly Jr, C. Allison, S. Garrett-Roe and S. A. Corcelli, Modeling carbon dioxide vibrational frequencies in ionic liquids: III. Dynamics and spectroscopy, *J. Phys. Chem. B*, 2018, **122**(38), 8931–8942.
62 C. Cadena, J. L. Anthony, J. K. Shah, T. I. Morrow, J. F. Brennecke and E. J. Maginn, Why is CO2 so soluble in imidazolium-based ionic liquids?, *J. Am. Chem. Soc.*, 2004, **126**(16), 5300–5308.
63 T. Brinzer, E. J. Berquist, Z. Ren, S. Dutta, C. A. Johnson, C. S. Krisher, D. S. Lambrecht and S. Garrett-Roe, Ultrafast vibrational spectroscopy (2D-IR) of CO2 in ionic liquids: Carbon capture from carbon dioxide's point of view, *J. Chem. Phys.*, 2015, **142**(21), 1–15.
64 K. Iida, D. Yokogawa, H. Sato and S. Sakaki, The barrier origin on the reaction of CO2+ OH− in aqueous solution, *Chem. Phys. Lett.*, 2007, **443**(4–6), 264–268.
65 B. Pinsent, L. Pearson and F. Roughton, The kinetics of combination of carbon dioxide with hydroxide ions, *Trans. Faraday Soc.*, 1956, **52**, 1512–1520.
66 J. M. P. Martirez and E. A. Carter, Solvent dynamics are critical to understanding carbon dioxide dissolution and hydration in water, *J. Am. Chem. Soc.*, 2023, **145**(23), 12561–12575.
67 S. Beer, M. Björk and J. Beardall, Carbon dioxide vs. bicarbonate utilisation, *Research methods of environmental physiology in aquatic sciences*, Springer, 2020, pp. 153–164.
68 O. Y. Gutiérrez, K. Grubel, J. Kothandaraman, J. A. Lopez-Ruiz, K. P. Brooks, M. E. Bowden and T. Autrey, Using earth abundant materials for long duration energy storage: electro-chemical and thermo-chemical cycling of bicarbonate/formate, *Green Chem.*, 2023, **25**(11), 4222–4233.
69 A. Yadav, R. M. Jackson, J. J. Holbrook and A. Warshel, Role of solvent reorganization energies in the catalytic activity of enzymes, *J. Am. Chem. Soc.*, 1991, **113**(13), 4800–4805.
70 M. Fuxreiter and L. Mones, The role of reorganization energy in rational enzyme design, *Curr. Opin. Chem. Biol.*, 2014, **21**, 34–41.
71 G. Norjmaa, J.-D. Maréchal and G. Ujaque, Microsolvation and encapsulation effects on supramolecular catalysis: C–C reductive elimination inside [Ga4L6] 12–metallocage, *J. Am. Chem. Soc.*, 2019, **141**(33), 13114–13123.
72 W.-L. Li, H. Hao and T. Head-Gordon, Optimizing the solvent reorganization free energy by metal substitution for Nanocage catalysis, *ACS Catal.*, 2022, **12**(7), 3782–3788.
73 R. R. Crichton, *Biological inorganic chemistry: a new introduction to molecular structure and function*, Elsevier, 2012.
74 N. J. Penders-van Elk, E. S. Hamborg, P. J. Huttenhuis, S. Fradette, J. A. Carley and G. F. Versteeg, Kinetics of absorption of carbon dioxide in aqueous amine and carbonate solutions with carbonic anhydrase, *Int. J. Greenhouse Gas Control*, 2013, **12**, 259–268.
75 N. J. Penders-van Elk, S. M. Oversteegen and G. F. Versteeg, Combined effect of temperature and pKa on the kinetics of absorption of carbon dioxide in aqueous alkanolamine and carbonate solutions with carbonic anhydrase, *Ind. Eng. Chem. Res.*, 2016, **55**(38), 10044–10054.
76 J. K. Yong, G. W. Stevens, F. Caruso and S. E. Kentish, The use of carbonic anhydrase to accelerate carbon dioxide capture processes, *J. Chem. Technol. Biotechnol.*, 2015, **90**(1), 3–10.
77 F. M. Perna, P. Vitale and V. Capriati, Deep eutectic solvents and their applications as green solvents, *Curr. Opin. Green Sustain. Chem.*, 2020, **21**, 27–33.
78 A. E. Ünlü, A. Arıkaya and S. Takaç, Use of deep eutectic solvents as catalyst: A mini-review, *Green Process Synth.*, 2019, **8**(1), 355–372.
79 N. Azizi, S. Dezfooli, M. Khajeh and M. M. Hashemi, Efficient deep eutectic solvents catalyzed synthesis of pyran and benzopyran derivatives, *J. Mol. Liq.*, 2013, **186**, 76–80.
80 Q. Wang, X. Yao, Y. Geng, Q. Zhou, X. Lu and S. Zhang, Deep eutectic solvents as highly active catalysts for the fast and mild glycolysis of poly (ethylene terephthalate)(PET), *Green Chem.*, 2015, **17**(4), 2473–2479.
81 X. Yang, Q. Zou, T. Zhao, P. Chen, Z. Liu, F. Liu and Q. Lin, Deep eutectic solvents as efficient catalysts for fixation of CO2 to cyclic carbonates at ambient temperature and pressure through synergetic catalysis, *ACS Sustain. Chem. Eng.*, 2021, **9**(31), 10437–10443.
82 B. Y. Man, J. M. Hook and J. B. Harper, Substitution reactions in ionic liquids. A kinetic study, *Tetrahedron Lett.*, 2005, **46**(44), 7641–7645.
83 Y.-Z. Zheng, H.-Y. He, Y. Zhou and Z.-W. Yu, Hydrogen-bonding interactions between [BMIM][BF4] and dimethyl sulfoxide, *J. Mol. Struct.*, 2014, **1069**, 140–146.
84 A. Y. Hsieh, R. S. Haines and J. B. Harper, Effects of Ionic Liquids on the Nucleofugality of Bromide, *J. Org. Chem.*, 2024, **89**(9), 6247–6256.
85 D. C. Morris, S. W. Prescott and J. B. Harper, Rapid relaxation NMR measurements to predict rate coefficients

in ionic liquid mixtures. An examination of reaction outcome changes in a homologous series of ionic liquids, *Phys. Chem. Chem. Phys.*, 2021, **23**(16), 9878–9888.
86 Z. Wen, Y. Wang, J. Yao and H. Li, Accelerated aerobic oxidative α-hydroxylation of 2-methylcyclohexanone with imidazolium ionic liquids, *Mol. Catal.*, 2023, **551**, 113630.
87 J. Alarcón-Espósito, R. Contreras, R. A. Tapia and P. R. Campodónico, Gutmann's donor numbers correctly assess the effect of the solvent on the kinetics of SNAr reactions in ionic liquids, *Chem. – Eur. J.*, 2016, **22**(37), 13347–13351.
88 B. J. Butler and J. B. Harper, The effect of the structure of the anion of an ionic liquid on the rate of reaction at a phosphorus centre, *J. Phys. Org. Chem.*, 2019, **32**(1), e3819.
89 A. Gilbert, R. S. Haines and J. B. Harper, The effects of using an ionic liquid as a solvent for a reaction that proceeds through a phenonium ion, *J. Phys. Org. Chem.*, 2021, **34**(9), e4217.
90 A. Gilbert, G. Bucher, R. S. Haines and J. B. Harper, Correlating ionic liquid solvent effects with solvent parameters for a reaction that proceeds through a xanthylium intermediate, *Org. Biomol. Chem.*, 2019, **17**(42), 9336–9342.
91 S. T. Keaveney, T. L. Greaves, D. F. Kennedy and J. B. Harper, Understanding the effect of solvent structure on organic reaction outcomes when using ionic liquid/acetonitrile mixtures, *J. Phys. Chem. B*, 2016, **120**(49), 12687–12699.
92 E. D. Kochly, A. M. Deh-Lee, N. J. Lemon, J. Rath and A. Escobar-Meza, The effect of ionic liquid cosolvents on a unimolecular solvolysis reaction in 2, 2, 2-trifluoroethanol, *Results Chem.*, 2021, **3**, 100213.
93 X. Zhang, X. Zhang, Z. Wen, Y. Wang, H. Li, K. Mochizuki and J. Yao, Key Roles of Free Cations in Modulating the Reaction Rate in Imidazolium Ionic Liquid–Dimethyl Sulfoxide Mixtures, *J. Phys. Chem. B*, 2024, **128**(41), 10200–10206.
94 S. Bishnoi and G. T. Rochelle, Absorption of carbon dioxide into aqueous piperazine: reaction kinetics, mass transfer and solubility, *Chem. Eng. Sci.*, 2000, **55**(22), 5531–5543.
95 J. T. Cullinane and G. T. Rochelle, Carbon dioxide absorption with aqueous potassium carbonate promoted by piperazine, *Chem. Eng. Sci.*, 2004, **59**(17), 3619–3630.
96 J. T. Cullinane and G. T. Rochelle, Kinetics of carbon dioxide absorption into aqueous potassium carbonate and piperazine, *Ind. Eng. Chem. Res.*, 2006, **45**(8), 2531–2545.
97 R. Lensen The promoter effect of piperazine on the removal of carbon dioxide, https://www.bsdfreaks.nl/files/hoofd6.pdf, 2004.
98 H. N. Po and N. Senozan, The Henderson-Hasselbalch equation: its history and limitations, *J. Chem. Educ.*, 2001, **78**(11), 1499.
99 G. Cui, M. Lv and D. Yang, Efficient CO 2 absorption by azolide-based deep eutectic solvents, *Chem. Commun.*, 2019, **55**(10), 1426–1429.
100 M. Costamagna, E. Micheli, V. Canale, M. Ciulla, G. Siani, P. Di Profio, M. Tiecco and G. Ciancaleoni, Low-cost temperature transition mixtures (TTM) based on ethylene glycol/potassium hydroxide as reversible CO2 sorbents, *J. Mol. Liq.*, 2021, **340**, 117180.
101 Y. Zhou, M. Chen, X. Dong and D. Yang, The Reaction between K2CO3 and Ethylene Glycol in Deep Eutectic Solvents, *Molecules*, 2024, **29**(17), 4113.
102 H. Yan, L. Zhao, Y. Bai, F. Li, H. Dong, H. Wang, X. Zhang and S. Zeng, Superbase ionic liquid-based deep eutectic solvents for improving CO2 absorption, *ACS Sustain. Chem. Eng.*, 2020, **8**(6), 2523–2530.
103 S. A. O. Restrepo and A. Adams, Fast quantification of water content in glycols by compact 1H NMR spectroscopy, *Talanta*, 2023, **253**, 123973.
104 J. Yoon, S. Yun, B. Kim, S. Ahn and K. Choi, Determination of water content in bioethanol using the 1H NMR chemical shift change, *Bull. Korean Chem. Soc.*, 2019, **40**(4), 313–316.
105 T. Loerting, C. Tautermann, R. T. Kroemer, I. Kohl, A. Hallbrucker, E. Mayer and K. R. Liedl, On the surprising kinetic stability of carbonic acid (H2CO3), *Angew. Chem., Int. Ed.*, 2000, **39**(5), 891–894.
106 J. Hegarty, B. Shindel, D. Sukhareva, M. L. Barsoum, O. K. Farha and V. Dravid, Expanding the Library of Ions for Moisture-Swing Carbon Capture, *Environ. Sci. Technol.*, 2023, **57**(50), 21080–21091.
107 J. S. Derrick, M. Loipersberger, S. K. Nistanaki, A. V. Rothweiler, M. Head-Gordon, E. M. Nichols and C. J. Chang, Templating bicarbonate in the second coordination sphere enhances electrochemical CO2 reduction catalyzed by iron porphyrins, *J. Am. Chem. Soc.*, 2022, **144**(26), 11656–11663.
108 P. Kortunov and M. Siskin, *Amine promotion for CO2 capture*, 2014.
109 M. Moradzaman and G. Mul, In situ Raman study of potential-dependent surface adsorbed carbonate, CO, OH, and C species on cu electrodes during electrochemical reduction of CO2, *ChemElectroChem*, 2021, **8**(8), 1478–1485.
110 H. Shu and Y. Xu, Tuning the strength of cation coordination interactions of dual functional ionic liquids for improving CO2 capture performance, *Int. J. Greenhouse Gas Control*, 2020, **94**, 102934.
111 J. Cheng, C. Wu, W. Gao, H. Li, Y. Ma, S. Liu and D. Yang, CO2 absorption mechanism by the deep eutectic solvents formed by monoethanolamine-based protic ionic liquid and ethylene glycol, *Int. J. Mol. Sci.*, 2022, **23**(3), 1893.
112 G. Luciano and R. Svoboda, Activation energy determination in case of independent complex kinetic processes, *Processes*, 2019, **7**(10), 738.
113 M. Menzinger and R. Wolfgang, The meaning and use of the Arrhenius activation energy, *Angew. Chem., Int. Ed. Engl.*, 1969, **8**(6), 438–444.
114 Z. A. Piskulich, O. O. Mesele and W. H. Thompson, Activation energies and beyond, *J. Phys. Chem. A*, 2019, **123**(33), 7185–7194.

115 A. Thorat, R. Sartape, R. Chauhan, R. Mishra, M. Singh and J. Shah, Ionic liquid-Enhanced Interfaces to Boost Reactive CO2 Capture, 2025.
116 L. Wang, X. Jin, P. Li, J. Zhang, H. He and S. Zhang, Hydroxyl-functionalized ionic liquid promoted CO2 fixation according to electrostatic attraction and hydrogen bonding interaction, *Ind. Eng. Chem. Res.*, 2014, **53**(20), 8426–8435.
117 Y. Wang, Y. Wang, Y. Zhao, J. Fu and Z. Liu, Ionic Liquids Promoted Transformation of Carbon Dioxide, *Chem. Rev.*, 2025, **125**, 6057–6129.
118 L. B. Hamdy, C. Goel, J. A. Rudd, A. R. Barron and E. Andreoli, The application of amine-based materials for carbon capture and utilisation: an overarching view, *Mater. Adv.*, 2021, **2**(18), 5843–5880.
119 C.-H. Yu, C.-H. Huang and C.-S. Tan, A review of CO2 capture by absorption and adsorption, *Aerosol Air Qual. Res.*, 2012, **12**(5), 745–769.
120 C. H. Giammanco, S. A. Yamada, P. L. Kramer, A. Tamimi and M. D. Fayer, Structural and rotational dynamics of carbon dioxide in 1-Alkyl-3-methylimidazolium bis (trifluoromethylsulfonyl) imide ionic liquids: The effect of chain length, *J. Phys. Chem. B*, 2016, **120**(27), 6698–6711.
121 A. Galvão and A. Francesconi, Solubility of methane and carbon dioxide in ethylene glycol at pressures up to 14 MPa and temperatures ranging from (303 to 423) K, *J. Chem. Thermodyn.*, 2010, **42**(5), 684–688.
122 J. Safarov, R. Hamidova, M. Stephan, N. Schmotz, I. Kul, A. Shahverdiyev and E. Hassel, Carbon dioxide solubility in 1-butyl-3-methylimidazolium-bis (trifluormethylsulfonyl) imide over a wide range of temperatures and pressures, *J. Chem. Thermodyn.*, 2013, **67**, 181–189.
123 R. M. Daniel and M. J. Danson, A new understanding of how temperature affects the catalytic activity of enzymes, *Trends Biochem. Sci.*, 2010, **35**(10), 584–591.
124 M. E. Peterson, R. M. Daniel, M. J. Danson and R. Eisenthal, The dependence of enzyme activity on temperature: determination and validation of parameters, *Biochem. J.*, 2007, **402**(2), 331–337.
125 R. Sardeing, P. Painmanakul and G. Hébrard, Effect of surfactants on liquid-side mass transfer coefficients in gas–liquid systems: a first step to modeling, *Chem. Eng. Sci.*, 2006, **61**(19), 6249–6260.
126 S. Zhang, D. Wang, F. Bu, X. Zhang and P. Fan, Gas–liquid mass transfer in the presence of ionic surfactant: effect of counter-ions and interfacial turbulence, *Surf. Interface Anal.*, 2013, **45**(7), 1152–1157.
127 F. Goodarzi and S. Zendehboudi, Effects of salt and surfactant on interfacial characteristics of water/oil systems: molecular dynamic simulations and dissipative particle dynamics, *Ind. Eng. Chem. Res.*, 2019, **58**(20), 8817–8834.
128 S. Hosseinpour, V. Götz and W. Peukert, Effect of surfactants on the molecular structure of the buried oil/water interface, *Angew. Chem., Int. Ed.*, 2021, **60**(47), 25143–25150.
129 J. J. Barker and R. E. Treybal, Mass transfer coefficients for solids suspended in agitated liquids, *AIChE J.*, 1960, **6**(2), 289–295.
130 R. E. Treybal, *Mass transfer operations*, New York, 1980, vol. 466, pp. 493–497.
131 J. Heijnen and K. Van't Riet, Mass transfer, mixing and heat transfer phenomena in low viscosity bubble column reactors, *Chem. Eng. J.*, 1984, **28**(2), B21–B42.
132 S. Ainsworth Michaelis-Menten kinetics, *Steady-state enzyme kinetics*, Springer, 1977, pp. 43–73.
133 A. Cornish-Bowden, One hundred years of Michaelis–Menten kinetics, *Perspect. Sci.*, 2015, **4**, 3–9.
134 M. Mezger, R. Roth, H. Schröder, P. Reichert, D. Pontoni and H. Reichert, Solid-liquid interfaces of ionic liquid solutions—Interfacial layering and bulk correlations, *J. Chem. Phys.*, 2015, **142**(16), 1–8.
135 G. Hebrard, J. Zeng and K. Loubiere, Effect of surfactants on liquid side mass transfer coefficients: a new insight, *Chem. Eng. J.*, 2009, **148**(1), 132–138.
136 P. Carvalho, K. Kurnia and J. Coutinho, Dispelling some myths about the CO2 solubility in ionic liquids, *Phys. Chem. Chem. Phys.*, 2016, **18**(22), 14757–14771.
137 M. J. Muldoon, S. N. Aki, J. L. Anderson, J. K. Dixon and J. F. Brennecke, Improving carbon dioxide solubility in ionic liquids, *J. Phys. Chem. B*, 2007, **111**(30), 9001–9009.